Battery Power Efficiency of PPM and FSK in Wireless Sensor Networks

Qiuling Tang, Liuqing Yang, *Member, IEEE,* Georgios B. Giannakis, *Fellow, IEEE,* and Tuanfa Qin

***Abstract*— As sensor nodes are typically powered by non-renewable batteries, energy efficiency is a critical factor in wireless sensor networks (WSNs). Orthogonal modulations appropriate for the energy-limited WSN setup have been investigated under the assumption that batteries are linear and ideal, but their effectiveness is not guaranteed when more realistic nonlinear battery models are considered. In this paper, based on a general model that integrates typical WSN transmission and reception modules with realistic battery models, we derive two battery power-conserving schemes for two M-ary orthogonal modulations, namely pulse position modulation (PPM) and frequency shift keying (FSK), both tailored for WSNs. Then we analyze and compare the battery power efficiency of PPM and FSK over various wireless channel models. Our results reveal that FSK is more power-efficient than PPM in sparse WSNs, while PPM may outperform FSK in dense WSNs. We also show that in sparse WSNs, the power advantage of FSK over PPM is no more than 3dB; whereas in very dense WSNs, the power advantage of PPM over FSK can be much more significant as the constellation size M increases.**

***Index Terms*— Wireless sensor networks (WSN), pulse position modulation (PPM), frequency shift keying (FSK), battery power efficiency, fading**

I. Introduction

WIRELESS sensor networks (WSNs) comprise a large number of sensor nodes, which are small in size, battery-powered and functioning autonomously (see e.g., [1]). Potential applications of WSNs include home networking, monitoring and surveillance, search-and-rescue operations in disaster areas, and tactical communications. The corresponding inter-node distance may vary from one meter to hundreds of meters. Because sensor nodes are typically powered by non-renewable batteries, energy efficiency is a critical factor in WSNs.

Manuscript received December 11, 2004; revised July 29 and December 4, 2005; accepted December 5, 2005. The associate editor coordinating the review of this letter and approving it for publication was R. Negi. Part of this work was presented at the *Milcom Conf.*, Atlantic City, NJ, Oct. 17-20, 2005. The work of the first and fourth authors was supported by the Science Research Foundation of Guangxi Education Department of China No. [2002]316. The work of the third author was supported by the NSF Grant No. EIA-0324864 and by the USDoD Army Grant No. W911NF-05-1-0283.

Q. Tang is with the Lab of Modern Acoustics, Nanjing University, Nanjing 210093, China; and with the College of Computer and Electronic Information, Guangxi University, Nanning 530004, China (e-mail: qiuling.tang@gmail.com).

L. Yang is with the Department of Electrical and Computer Engineering, University of Florida, Gainesville, FL 32611, USA (e-mail: lqyang@ece.ufl.edu).

G. B. Giannakis is with the Department of Electrical and Computer Engineering, University of Minnesota, Minneapolis, MN 55455, USA (e-mail: georgios@ece.umn.edu).

T. Qin is with the Lab of Modern Acoustics, Nanjing University, Nanjing 210093, China; and with the College of Computer and Electronic Information, Guangxi University, Nanning 530004, China (e-mail: tfqin@gxu.edu.cn).

Digital Object Identifier 10.1109/LCOMM.2007.04851.

Several energy-efficient approaches have been investigated, including network protocols [3] as well as cross-layer designs [4]. At the physical layer, modulation, coding, adaptive resource allocation, and cooperative relays have been pursued to effect energy efficiency in the overall system performance; see e.g., [7], [13], [17]. However, all are built on the premise that the power-supplying batteries are ideal and linear. This implies that the battery power consumption equals the total power required by all energy-consuming modules, including signal processing, hardware circuitry and transmitter modules. In fact, part of the battery's capacity (stored energy) may be wasted during its discharge process. For this reason, the lifetime of battery-driven sensor nodes depends not only on the power required by energy-consuming modules, but also on the unique nonlinear characteristics of batteries. Realistic nonlinear battery models are available [11], [15], and have been considered in the rapidly evolving area of battery-driven system design. Compared to conventional low power designs, the latter has the potential to markedly improve the lifetime of battery-powered systems [6]. However, existing battery-driven approaches have so far dealt with hardware and software optimization of a single node [9], [11], or, routing aspects of energy-constrained networks [16]; but not with modulation and communication issues at the physical layer. There is clearly a need to integrate available battery models in the design and evaluation of modulation and communication schemes for WSNs.

To this end, the present paper explores battery-driven issues for low power modulations. We derive a general model that integrates typical WSN transmission and reception modules with realistic battery models capturing the nonlinear relationship between battery capacity and variations of the discharge current profile. The latter distinguishes our model from existing alternatives [2], [13], [17]. Compared with cellular networks, WSNs can be deployed more densely so that the corresponding transmit power is considerably smaller and may be comparable to or even be much smaller than circuit power consumption. On the other hand, data rates in most WSNs are low and complex signal processing operations are not desirable. For this reason, our general model views power consumption for signal processing operations as negligible and focuses on analog circuit power consumption. Using this model, we evaluate the power efficiency of two orthogonal modulations: pulse position modulation (PPM) and frequency shift keying (FSK)[1]. As power efficiency is intimately related to nonlinear battery

[1]Up to date, FSK is more commonly employed in wireless communications and has been chosen for the MICA2 Motes (see e.g., [12]; whereas PPM is generally adopted in optical communications. Only recently PPM began to gain growing attention in the emerging field of Ultra-wideband (UWB) wireless technologies.

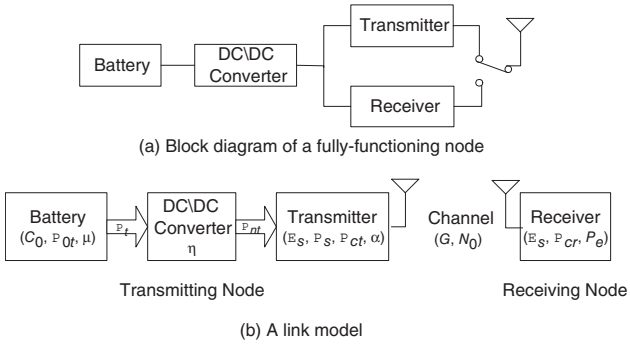

Fig. 1. System model.

models, we term it *battery power efficiency*. We quantify the battery power efficiency of PPM and FSK for sparse and dense WSNs, over path-loss and fading wireless channels. Our analysis and comparisons suggest that different sensor densities and data rates favor different modulation schemes. While ensuring low-power operation of sensor nodes, our model is also unique in that it includes non-coherent detection and energy-efficient circuit work/sleep modes.

The remainder of this paper is organized as follows. In the following section, we put forward our general system model for battery-driven sensors. In Section III, we specify the modulation, transmission and detection schemes, and transceiver circuit structure for PPM and FSK. Then we analyze and compare their battery power efficiencies in various channel models in Section IV. Finally, we provide numerical results for our analysis in Section V and concluding remarks in Section VI.

II. General System Model

To facilitate subsequent analysis and comparisons, we build in this section a general system model for a single battery-driven node in transmit- or receive-mode. The system model will account for battery power efficiency, direct current to direct current (DC/DC) converter power transfer, power consumption in signal transmission, power consumption of transceiver circuitry, modulation type and size, as well as path loss and fading effects of wireless propagation channels.

The diagram of a node is shown in Fig. 1(a), which includes a transmitter, a receiver, a power-supporting battery and a DC/DC converter to generate a desired and stable supply voltage for the transmitter or the receiver. The node works in a half-duplex communication mode (alternately transmitting and receiving), which is commonly used in WSNs for power efficiency. To explore the battery power consumption at the node, we will consider a point-to-point link in the network. This link consists of a transmitting node and a receiving node, where only the transmitter in the former and the receiver in the later are switched on. Based on the link model shown in Fig. 1(b), we will figure out the battery power consumption in the transmitting node and receiving node respectively, and then we will integrate them to assess the battery power consumption of the fully-functioning node.

Let us consider the transmitting node first. To achieve a prescribed symbol error rate (SER) that satisfies quality of service (QoS) requirements, a symbol energy $\mathcal{E}_d$ is needed at the receiver. The corresponding symbol energy at the transmitter $\mathcal{E}_s$ is $\mathcal{E}_s = \mathcal{E}_d/G$, where G is the channel gain which captures the channel effects, and can be either constant (AWGN channels) or varying (over distance d in path-loss channels or over time in fading channels). With a rectangular pulse shaper of duration T_p, the transmit power is $\mathcal{P}_s = \mathcal{E}_s/T_p$. In WSNs, circuit power consumption $\mathcal{P}_{ct}$ in the transmitting node may be comparable to transmit power $\mathcal{P}_s$ and needs to be considered too. Hence, the total power consumption at the transmitter $\mathcal{P}_{nt}$ is given by

$$\mathcal{P}_{nt} = (1+\alpha)\mathcal{P}_s + \mathcal{P}_{ct}, \tag{1}$$

where $\alpha\mathcal{P}_s$ $(0 < \alpha < 1)$ corresponds to the power consumed by the power amplifier. Factor $\alpha = \xi/\varsigma - 1$ depends on the drain efficiency ς of the RF power amplifier and the peak-to-average power ratio (PAPR) ξ of the transmitted signal. For constant modulus modulations, we have $\xi = 1$; and for class-B power amplifiers not limited to operate in the linear region, the drain efficiency is $\varsigma = 0.75$. For convenience, we will henceforth call $(1+\alpha)\mathcal{P}_s$ the total transmit power.

As the supply voltage required by the transmitter circuits can be different from the battery voltage V, a power-consuming DC/DC converter is needed. Therefore, to provide the total power $\mathcal{P}_{nt}$ at the transmitting node, the power drawn from the battery (discharge power) is $\mathcal{P}_t = \frac{\mathcal{P}_{nt}}{\eta}$, where $\eta < 1$ is the transfer efficiency of the DC/DC converter. If the battery is linear, then its power consumption is identical to its discharge power. However, batteries are generally nonlinear and part of their stored energy (capacity) is wasted when they release energy to drive the transmitter. Nonlinearities are known to manifest themselves as rate capacity and recovery effects [10]. If the discharge current is small, the stored energy will be completely used or released. In this case, the battery can be considered as linear. But if the discharge current has large magnitude, nonlinearities emerge and a considerable portion of the stored energy is wasted. The amount of wasted energy heavily depends on the discharge current profile. This is known as rate capacity effect. Furthermore, if a battery is discharged intermittently, i.e., every discharge interval is followed by an idle period, the amount of energy delivered increases, since the battery can partially recover the capacity wasted in the previous discharges during idle periods. This is known as recovery effect. Relative to the recovery effect, the rate capacity effect influences more critically battery capacity [9]. For this reason, we will consider only the rate capacity effect in our model.

Let C_0 denote the capacity of a new battery, defined as the total energy it stores. It is related to the energy C actually consumed by the source node through the so-termed battery efficiency factor: $\mu := C/C_0$. Accordingly, the actual power used in the battery is $\mathcal{P}_t/\mu = VI_t/\mu$, where V and I_t are the discharge voltage and current during a pulse interval. Corroborated with experiments, two models are available to describe the relationship between discharge current and efficiency [11]

$$\mu(I_t) = 1 - \omega I_t, \tag{2}$$

$$\text{and} \quad \mu(I_t) = 1 - \nu I_t^2, \tag{3}$$

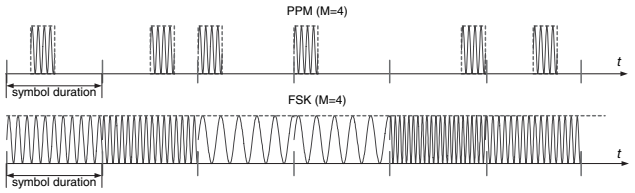

Fig. 2. Transmit current waveforms for PPM and FSK with $M = 4$.

where ω and ν are both positive constants. The battery efficiency factor μ varies from $\mu_{\max}$ to $\mu_{\min}$ when the discharge current increases from the rated minimum $I_{\min}$ to the rated maximum $I_{\max}$. Generally, $\mu_{\max} = 1$ and $\mu_{\min}$ can be as small as 0.5 [11].

Let us consider the discharge current waveforms in a low-data-rate WSN, which are similar to the transmit current profiles shown in Fig. 2. If i_t denotes the instantaneous discharge current with probability density function (pdf) $f(i_t)$, the actual power consumption of the battery is $Vi_t/\mu(i_t)$. It follows that the average actual power consumption (AAPC) of the battery can be expressed as

$$\mathcal{P}_{0t} = V \int_{I_{\min}}^{I_{\max}} \frac{i_t}{\mu(i_t)} f(i_t)\, di_t. \tag{4}$$

The important implication of this expression is that even with the same battery parameters (ω or ν), different modulation schemes and circuit operation modes will give rise to different $f(i_t)$'s and thus different battery AAPCs. For a fixed current mean value $E\{i_t\}$, the minimum battery AAPC $\mathcal{P}_{0t}$ occurs when i_t follows a single δ-function distribution and $\mathcal{P}_{0t}$ is maximized when i_t is uniformly distributed [11].

As for the receiving node, assuming it is powered by a battery through a DC/DC converter with the same parameters as those for the transmitting node, the aforementioned battery power consumption model for transmitting node can be used for the receiving node after replacing the total power consumption expression (1) for the transmitter with $\mathcal{P}_{nr} = \mathcal{P}_{cr}$ for the receiver. This is possible because there is no transmit power and only the circuit power consumption needs to be considered at the receiving node. It is worth mentioning that the variables about power and discharge current of the receiving node are distinguished by a subscript 'r' from those for the transmitting node which have a subscript 't'.

Having obtained the AAPCs for the transmitting node and the receiving node, the battery AAPC for the fully-functioning node is

$$\mathcal{P}_0 = a\mathcal{P}_{0t} + (1-a)\mathcal{P}_{0r}, \tag{5}$$

where the factor $0 < a < 0.5$ because a node generally listens longer time than it transmits in order to reduce the aggregate interference in the network.

With battery capacity C_0 and AAPC $\mathcal{P}_0$, the battery lifetime is $C_0/\mathcal{P}_0$. Obviously, smaller $\mathcal{P}_0$ implies longer battery lifetime. Therefore, battery AAPC $\mathcal{P}_0$ measures battery power efficiency.

So far, we have established a general battery-driven system model. Based on this model, we will evaluate the battery power efficiency of two orthogonal modulations.

III. Battery-Aware PPM and FSK Schemes

In this section, we rely on power-efficient orthogonal modulations to derive battery power-conserving schemes tailored for WSNs. Our schemes use non-coherent detection and take into account power-efficient circuit work/sleep operating modes, carrier/baseband transmissions, low power low-IF transceiver design, and the nonlinear battery models we outlined in the previous section.

Frequency shift keying (FSK) is a widely adopted orthogonal modulation. The recent emergence of (ultra-)wideband carrier-free signaling has also spurred renewed interest in pulse position modulation (PPM), another common orthogonal modulation. For a given bandwidth B, the rectangular transmitted current waveforms corresponding to PPM and FSK are depicted in Fig. 2. With M-ary PPM and symbol period T_s, the pulse duration is $T_p = T_s/M \approx 1/B$ and the bandwidth efficiency is $B_e = R_b/B = k/(T_sB) \approx k/M$, where $k = \log_2 M$ is the number of bits per symbol. The frequency separation for M-ary FSK is $\Delta f = B/M$ and the pulse duration $T_p \approx 1/\Delta f = M/B$. Since FSK entails no idle interval, the symbol period is $T_s = T_p$, which gives rise to the same bandwidth efficiency $B_e \approx k/M$ as PPM. As the constellation size M increases, bandwidth efficiency B_e decreases, but the required energy for transmitting a bit also decreases for any preset error probability. The price paid for this power efficiency is longer symbol duration in PPM and larger bandwidth in FSK. In fact, PPM and FSK can be considered as dual since the former relies on "spiky" signalling in the time domain whereas the latter relies on "spiky" signalling in the frequency domain.

We will consider FSK with carrier transmission, and PPM with carrier/carrier-less transmission. Being orthogonal, both FSK and PPM can afford low-complexity non-coherent detection and yield the same SER performance. Non-coherent detection typically refers to signal demodulation in the presence of unknown carrier phase. In our setup, however, its meaning is more general. The term "non-coherent detection" will refer to demodulation without knowledge of the fading channel, including the phase and amplitude of the fading coefficient. In the carrier-based mode, the unknown phase can be random on $[0, 2\pi)$; whereas in the carrier-less case, the unknown phase can be either 0 or π. In this broader sense, the non-coherent receivers corresponding to FSK and PPM will both be energy detectors, one in the frequency domain and the other in the time domain. Hence, the same SER formula can be used for both of them.

As far as SER is concerned, lack of closed form expressions for a general M motivates upper bounds closely approximating the SER of M-ary FSK and M-ary PPM at medium-to-high SNR. To this end, the union bound is well-known and widely adopted; see also [5] for a tighter bound but with coherent detection. Here, we establish upper bounds for M-ary orthogonal modulations with non-coherent detection over various channels (see Appendix I for the proof):

Lemma 1: *If G denotes the channel gain and N_0 the spectral density of the AWGN, the instantaneous SER for M-ary orthogonal signaling in AWGN with non-coherent detection*

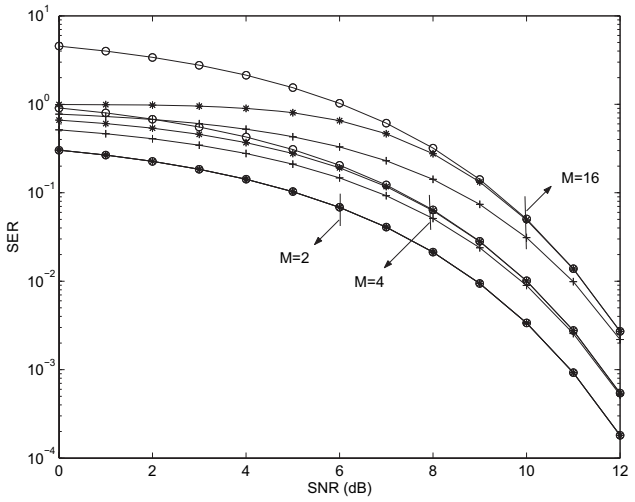

Fig. 3. SER performance comparisons among the union bounds (circle), our upper bounds (cf. (6)) (asterisk) and the theoretical results (plus sign) with M =2, 4, 16.

is upper-bounded by

$$P_e \leq 1 - \left(1 - 0.5e^{-\frac{1}{2}G\frac{\mathcal{E}_s}{N_0}}\right)^{M-1} . \tag{6}$$

This bound is universally tighter than the union bound $\forall \mathcal{E}_s/N_0$ *and* $\forall M$ *but* $M = 2$.

Comparisons among the theoretical result in [14, Chap. 5], the union bound, and our bound in Lemma 1 are depicted in Fig. 3 which shows that our bound performs *universally* better than the widely-adopted union bound, especially at low-to-medium SNR. As confirmed by the simulations in Fig. 3, our SER bound is very close to the true SER. For this reason, we will henceforth use this bound in lieu of the true SER.

Based on Lemma 1, the transmit energy per symbol for any prescribed SER P_e in AWGN and path-loss channels is approximately:

$$\mathcal{E}_s = 2N_0 G^{-1} \ln\left(2\left(1 - (1 - P_e)^{\frac{1}{M-1}}\right)\right)^{-1}. \tag{7}$$

In fading channels, however, the average SER needs to be considered (see Appendix II for the proof):

Lemma 2: *In Rayleigh fading channels,* $\bar{G} := \mathrm{E}\{G\}$*, the average SER for* M*-ary orthogonal signaling with non-coherent detection is upper bounded by*

$$\bar{P}_e \leq 1 - \left(1 - \frac{1}{2 + \bar{G}\frac{\mathcal{E}_s}{N_0}}\right)^{M-1}, \quad \forall M, \quad \mathcal{E}_s/N_0 . \tag{8}$$

Using Lemma 2, the transmit energy per symbol for any prescribed average SER in Rayleigh fading channels is approximately

$$\mathcal{E}_s = N_0 \bar{G}^{-1}\left(\left(1 - (1 - \bar{P}_e)^{\frac{1}{M-1}}\right)^{-1} - 2\right). \tag{9}$$

Eqs. (7) and (9) can be readily applied to PPM and FSK for path-loss and Rayleigh fading channels respectively.

Based on a generic low-intermediate frequency (low-IF) transceiver structure, both FSK and PPM with carrier transmission adhere to a similar analog circuit model. On the other hand, baseband processing, e.g. source coding, pulse-shaping and modulation at the transmitter, and low-IF processing, e.g. demodulation, envelop detection and decision at the receiver, can be implemented digitally. The associated power consumption is much smaller compared with the power consumption in the radio frequency (RF) circuit with low data rate and low-complexity signal processing algorithms. Therefore, we neglect the power consumption in the digital logic parts and focus on the analog circuitry. The analog circuit model is shown in Fig. 4. At the FSK transmitter, the signal is modulated by switching on different control voltages for a voltage control oscillator (VCO) to generate the required radio frequencies. For PPM, a VCO is also needed to carry out the carrier modulation. After modulation, the RF signal waveform is amplified and transmitted. At the receiver, the received RF signal is first converted to an IF signal, then demodulated and envelop-detected in the baseband digitally. Specifically, the received RF signal is first filtered by a frontend filter and amplified by a low noise amplifier (LNA); after cleaned by an anti-aliasing filter, it is down-converted by a mixer; then filtered again, it goes through the IF amplifier (IFA) whose gain is adjustable; finally it is converted to a digital signal via the analog-to-digital converter (ADC), after which demodulation and processing are performed digitally. Based on this circuit model, the power consumption at the transmitter $\mathcal{P}_{ct}$ is

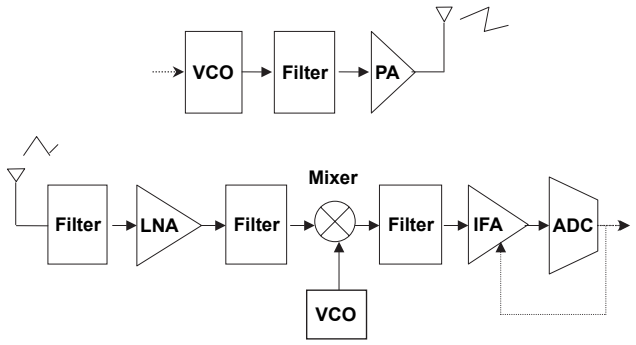

Fig. 4. Transceiver analog circuit blocks.

$$\mathcal{P}_{ct} = \mathcal{P}_{LO} + \mathcal{P}_{filt} \tag{10}$$

and at the receiver

$$\mathcal{P}_{cr} = \mathcal{P}_{LO} + \mathcal{P}_{mix} + \mathcal{P}_{LNA} + \mathcal{P}_{filr} + \mathcal{P}_{IFA} + \mathcal{P}_{ADC}, \tag{11}$$

where $\mathcal{P}_{LO}$ is the power consumption of VCO and $\mathcal{P}_{filt}$ is that of the filter at the transmitter. $\mathcal{P}_{mix}$, $\mathcal{P}_{LNA}$, $\mathcal{P}_{filr}$, $\mathcal{P}_{IFA}$ and $\mathcal{P}_{ADC}$ denote the powers consumed in the mixer, LNA, filter, IFA and ADC at the receiver, respectively. As to the carrier-less PPM scheme, compared with the analog circuit model in Fig.4, the VCO at the transmitter will be replaced by a pulse generator, which is triggered by the digitally-modulated signal to produce the baseband PPM signal waveform. At the receiver, the VCO and the mixer should also be removed.

So far, we have seen that PPM and FSK share the same bandwidth efficiency and SER performance, and a similar RF transceiver structure. However, Fig. 2 testifies that their transmitted signals are quite different. This difference implies distinct circuit operating modes, discharge current pdfs and

thereby battery AAPC's. These differences can be summarized as follows:

1. To achieve a given SER P_e (or $\bar{P}_e$), PPM and FSK require identical transmit energy per symbol. Hence, the transmit powers for PPM ($\mathcal{P}_s^p$) and FSK ($\mathcal{P}_s^f$) are related via: $\mathcal{P}_s^p(M) = M\mathcal{P}_s^f(M)$, simply because $T_p = T_s/M$ with PPM, and $T_p = T_s$ with FSK. Recall that the superscripts 'p' and 'f' are used to distinguish the variables for PPM and FSK, respectively.
2. As to circuit power consumption, differences arise in their circuit operating modes. Because PPM has active and idle intervals, by turning on and off the circuits according to the transmission state, we consider here a sleep mode during idle intervals at both transmitter and receiver. On the other hand, FSK is always in an active mode. This difference will turn out to have major impact in the battery power efficiency comparisons that we will pursue in the next section.
3. Their discharge current pdfs are different:
$$\begin{array}{ll} f(i^p) = \frac{1}{M}\delta(i^p - I^p) + \frac{M-1}{M}\delta(i^p), & \text{for PPM,} \\ f(i^f) = \delta(i^f - I^f), & \text{for FSK,} \end{array} \tag{12}$$
where i^p and i^f are the discharge currents for PPM and FSK, and I^p and I^f are their corresponding values in active mode. The pdfs can be used in both the transmitting node and the receiving node by adding their corresponding subscripts 't' and 'r' to the current variables in (12). Due to the dependence of $\mu(i)$ on $f(i)$ (cf. (4)), the different pdfs will result in different battery power efficiencies for PPM and FSK.
4. In addition to their distinct operating modes, the circuit power consumptions for FSK and PPM are also different because their components and devices are not identical. The difference at the transmitter is captured by a factor θ_t with $\mathcal{P}_{ct}^p = \theta_t\mathcal{P}_{ct}^f$ and commonly $\theta_t < 1$. Similarly, we also use a proportionality factor θ_r to describe the difference between the circuit power consumptions for FSK ($\mathcal{P}_{cr}^f$) and PPM ($\mathcal{P}_{cr}^p$) at the receiver with $\mathcal{P}_{cr}^p = \theta_r\mathcal{P}_{cr}^f$, and $\theta_r < 1$.

Summarizing, both FSK and PPM are power-efficient modulations. Both can afford low-complexity non-coherent detection and have a similar RF transceiver structure. While PPM enables sleep mode during idle intervals, FSK enjoys the optimal discharge current distribution: a single δ function, which minimizes the battery AAPC if the mean of the discharge current remains invariant.

To facilitate battery power efficiency comparison between the two modulation schemes, we define the ratio of their corresponding AAPCs as battery power efficiency ratio (BPER)

$$R_e := 10\log\left(\mathcal{P}_0^p/\mathcal{P}_0^f\right). \tag{13}$$

In the ensuing sections, we will quantify R_e for different wireless propagation channels.

IV. Battery Power Efficiency Comparisons

Substituting our results in Section III into the system model that we established in Section II, at the transmitting node, the transmit powers of PPM and FSK can be expressed in terms of their transmit energy per symbol as (cf. (7) and (9)):

$$\begin{array}{ll} \mathcal{P}_s^p = \frac{\mathcal{E}_s}{T_p} = \mathcal{E}_s B, & \text{for PPM,} \\ \mathcal{P}_s^f = \frac{\mathcal{E}_s}{T_s} = \frac{\mathcal{E}_s B}{M}, & \text{for FSK.} \end{array} \tag{14}$$

Setting the circuit power consumption for FSK $\mathcal{P}_{ct}^f = \mathcal{P}_{ct}$, it follows that the total power consumption at the transmitter module is

$$\begin{array}{ll} \mathcal{P}_{nt}^p = \mathcal{E}_s\beta + \theta_t\mathcal{P}_{ct}, & \text{for PPM,} \\ \mathcal{P}_{nt}^f = \frac{\mathcal{E}_s\beta}{M} + \mathcal{P}_{ct}, & \text{for FSK,} \end{array}$$

where $\beta := (1+\alpha)B$ for convenience. Their corresponding discharge currents in active mode can then be expressed as

$$\begin{array}{ll} I_t^p = \frac{1}{V\eta}\left(\mathcal{E}_s\beta + \theta_t\mathcal{P}_{ct}\right), & \text{for PPM,} \\ I_t^f = \frac{1}{V\eta}\left(\frac{\mathcal{E}_s\beta}{M} + \mathcal{P}_{ct}\right), & \text{for FSK.} \end{array} \tag{15}$$

Substituting (12) and (15) into (4), the battery AAPCs at the transmitting node can be obtained as

$$\begin{array}{ll} \mathcal{P}_{0t}^p = \frac{1}{\eta}\cdot\frac{\mathcal{E}_s\beta+\theta_t\mathcal{P}_{ct}}{M}\cdot\frac{1}{\mu(I_t^p)}, & \text{for PPM,} \\ \mathcal{P}_{0t}^f = \frac{1}{\eta}\cdot\left(\frac{\mathcal{E}_s\beta}{M} + \mathcal{P}_{ct}\right)\cdot\frac{1}{\mu(I_t^f)}, & \text{for FSK.} \end{array} \tag{16}$$

As for the receiving node, owing to no transmit power and letting the circuit power consumption for FSK be $\mathcal{P}_{cr}^f = \mathcal{P}_{cr}$, the total power consumption in the receiver module is

$$\mathcal{P}_{nr}^p = \theta_r\mathcal{P}_{cr}, \quad \text{for PPM,} \quad \text{and} \quad \mathcal{P}_{nr}^f = \mathcal{P}_{cr}, \quad \text{for FSK.}$$

Similarly, with the associated discharge currents

$$I_r^p = \frac{\theta_r\mathcal{P}_{cr}}{V\eta}, \quad \text{for PPM,} \quad \text{and} \quad I_r^f = \frac{\mathcal{P}_{cr}}{V\eta}, \quad \text{for FSK,}$$

and their pdfs expressed in (12), we can derive the battery AAPCs to be that

$$\begin{array}{ll} \mathcal{P}_{0r}^p = \frac{1}{\eta}\cdot\frac{\theta_r\mathcal{P}_{cr}}{M}\cdot\frac{1}{\mu(I_t^p)}, & \text{for PPM,} \\ \mathcal{P}_{0r}^f = \frac{1}{\eta}\cdot\mathcal{P}_{cr}\cdot\frac{1}{\mu(I_r^f)}, & \text{for FSK.} \end{array} \tag{17}$$

Accordingly, for a node operating in a half-duplex communication mode, the battery AAPCs for PPM and FSK are obtained from (5) as

$$\begin{aligned} \mathcal{P}_0^p &= \frac{a}{\eta M}\cdot\left((\mathcal{E}_s\beta + \theta_t\mathcal{P}_{ct})\cdot\frac{1}{\mu(I_t^p)} + \frac{1-a}{a}\cdot\theta_r\mathcal{P}_{cr}\cdot\frac{1}{\mu(I_r^p)}\right), \\ \mathcal{P}_0^f &= \frac{a}{\eta M}\cdot\left((\mathcal{E}_s\beta + M\mathcal{P}_{ct})\cdot\frac{1}{\mu(I_t^f)} + \frac{1-a}{a}\cdot M\mathcal{P}_{cr}\cdot\frac{1}{\mu(I_r^f)}\right). \end{aligned} \tag{18}$$

Then, by the definition of BPER, we have

$$R_e = 10\log\left(\frac{(\mathcal{E}_s\beta + \theta_t\mathcal{P}_{ct})\cdot\frac{1}{\mu(I_t^p)} + \frac{1-a}{a}\cdot\theta_r\mathcal{P}_{cr}\cdot\frac{1}{\mu(I_r^p)}}{(\mathcal{E}_s\beta + M\mathcal{P}_{ct})\cdot\frac{1}{\mu(I_t^f)} + \frac{1-a}{a}\cdot M\mathcal{P}_{cr}\cdot\frac{1}{\mu(I_r^f)}}\right). \tag{19}$$

Evidently, FSK is more battery power-efficient if $R_e > 0$, and vice versa. In the ensuing subsections, we will evaluate R_e for path-loss and Rayleigh fading channels. The density of WSNs determines the average inter-sensor distance d and thus the transmit power $\mathcal{P}_s$, which is proportional to d^k in K^{th}-power path-loss channel and may vary $2K$ orders depending on d which may vary from a few meters to a few hundred meters. Since the circuit power consumption remains approximately constant irrespective of d, we define as sparse WSNs those for which $\mathcal{P}_s \gg \mathcal{P}_{ct}$ and $\mathcal{P}_s \gg \mathcal{P}_{cr}$; otherwise, we term them

dense. In the former scenario, the circuit power consumption is much smaller than the transmit power and is thus negligible; whereas in the latter scenario, the circuit power consumption cannot be neglected.

A. Path-Loss Channel

For a K^{th}-power path-loss channel, the gain factor G_d depends on the transceiver distance d and is given by $G_d = \mathcal{P}_s/\mathcal{P}_d = M_l d^K G_1$, where the link margin M_l accounts for the effects of transceiver hardware, residual additive background interference, and G_1 is the gain factor at $d = 1$ which is specified by the antenna gain, carrier frequency and other system parameters. With $G = 1/G_d$, the transmit energy per symbol in Eq. (7) is a function of both M and d:

$$\mathcal{E}_s(M,d) = 2N_0 M_l G_1 d^K \cdot \ln\left(2\left(1-(1-P_e)^{\frac{1}{M-1}}\right)\right)^{-1}. \tag{20}$$

Hence, the corresponding discharge currents, battery AAPC and BPER all are functions of M and d. Additionally, we prove in Appendix III the following properties for $\mathcal{E}_s(M,d)$:

Lemma 3: *The required energy per symbol in path-loss channels $\mathcal{E}_s(M,d)$ is a monotonically increasing function of M, $\forall P_e$; while $\mathcal{E}_s(M,d)/M$ is a monotonically decreasing function of M for the practical SER range $P_e \leq 0.0677$.*

With Lemma 3, we are now ready to compare the battery power efficiency of PPM and FSK for sparse and dense WSNs. For a clear development, we start with the sparse case.

A.1. Sparse WSNs: When the circuit power consumption is considered to be negligible compared with the transmit power, i.e., when $\mathcal{P}_{ct} = 0$ and $\mathcal{P}_{cr} = 0$, the battery AAPCs in (18) turn out to be

$$\begin{aligned} \mathcal{P}_0^p(M,d) &= \tfrac{1}{2\eta}\tfrac{\mathcal{E}_s(M,d)\beta}{M}\tfrac{1}{\mu(I_t^p(M,d))}, \quad \text{for PPM,} \\ \mathcal{P}_0^f(M,d) &= \tfrac{1}{2\eta}\tfrac{\mathcal{E}_s(M,d)\beta}{M}\tfrac{1}{\mu(I_t^f(M,d))}, \quad \text{for FSK,} \end{aligned} \tag{21}$$

where the discharge current $I_t^p(M,d)$ and $I_t^f(M,d)$ can be obtained from (15) as

$$\begin{aligned} I_t^p(M,d) &= \tfrac{\mathcal{E}_s(M,d)\beta}{V\eta}, \quad \text{for PPM,} \\ I_t^f(M,d) &= \tfrac{\mathcal{E}_s(M,d)\beta}{MV\eta}, \quad \text{for FSK.} \end{aligned} \tag{22}$$

Then, the resulting BPER is that

$$R_e(M,d) = 10\log\left(\frac{\mu(I_t^f(M,d))}{\mu(I_t^p(M,d))}\right). \tag{23}$$

Evaluating $R_e(M,d)$, we obtain the following result.

Proposition 1: *In sparse WSNs over pass-loss channels, where the circuit power consumption is neglected, the following results hold true:*

i) *FSK is more battery power-efficient than PPM $\forall M$ and $\forall d$.*
ii) *For a fixed d, the power advantage of FSK over PPM increases as M increases.*
iii) *For a fixed M, the power advantage of FSK over PPM increases as d increases.*
iv) *The advantage of FSK over PPM is at most 3dB; that is, $\max\{R_e(M,d)\} < 3dB$, $\forall M, d$.*

Proof: see Appendix IV.

The intuition behind Proposition 1 can be obtained from the discharge current pdfs and their average values for PPM and FSK. According to the system model in Section II, to achieve a given SER P_e in path-loss channels, the average transmit power for PPM and FSK is identically equal to $\bar{p}_s^p = \bar{p}_s^f = \mathcal{E}_s/T_s$. With $\mathcal{P}_{ct} = 0$ and $\mathcal{P}_{cr} = 0$, the battery discharge powers only rely on the transmit power so that their average discharge powers are also the same $\bar{p}_t^p = \bar{p}_t^f$. As $p_t = Vi_t$, the mean values of their discharge currents obey $\bar{i}_t^p = \bar{i}_t^f$. However, the FSK discharge current i_t^f has the optimal distribution function: a single δ function, which leads to a higher power efficiency.

It appears from Proposition 1 that one should always prefer FSK $\forall M, d$. But if the circuit power consumption is taken into account, we will arrive at a different conclusion.

A.2. Dense WSNs: When the circuit power consumption $\mathcal{P}_{ct} \neq 0$ and $\mathcal{P}_{cr} \neq 0$, the corresponding battery discharge currents, battery AAPCs and BPER have all been presented at the beginning of this section; see Eqs. (15) to (18). In fact, when a node operates as a receiver and there is only circuit power consumption, the battery generally discharges linearly, that is:

$$\mu(I_r^p(M,d)) \approx \mu_{\max}, \quad \text{and} \quad \mu(I_r^f(M,d)) \approx \mu_{\max}. \tag{24}$$

Hence, we can rewrite (19) as

$$\begin{aligned} &R_e(M,d) \\ &= 10\log\left(\frac{(\mathcal{E}_s(M,d)\beta+\theta_t\mathcal{P}_{ct})\cdot\frac{1}{\mu(I_t^p(M,d))}+\frac{1-a}{a}\cdot\theta_r\mathcal{P}_{cr}\cdot\frac{1}{\mu_{\max}}}{(\mathcal{E}_s(M,d)\beta+M\mathcal{P}_{ct})\cdot\frac{1}{\mu(I_t^f(M,d))}+\frac{1-a}{a}\cdot M\mathcal{P}_{cr}\cdot\frac{1}{\mu_{\max}}}\right). \end{aligned} \tag{25}$$

When $\mathcal{P}_{ct} = 0$ and $\mathcal{P}_{cr} = 0$, $R_e(M,d)$ simplifies to (23) and is positive. But at the transmitter, as $\mathcal{P}_{ct}$ increases, the discharge currents I_t^p and I_t^f in (15) increase by the same order of magnitude and so do the battery AAPCs $\mathcal{P}_{0t}^p$ and $\mathcal{P}_{0t}^f$ in (16). Pdfs of the discharge currents i_t^p and i_t^f in (12) indicate that the mean $\bar{i}_t{}^f$ increases more rapidly than $\bar{i}_t{}^p$. Consequently, $\mathcal{P}_{0t}^f$ increases more rapidly than $\mathcal{P}_{0t}^p$. Also at the receiver, Eqs. (17) and (24) show that $\mathcal{P}_{0r}^f \geq \mathcal{P}_{0r}^p, \forall M$ and their difference rises when $\mathcal{P}_{cr}$ increases. It is expected that, when circuit power $\mathcal{P}_{ct}$ and $\mathcal{P}_{cr}$ exceeds certain values, $\mathcal{P}_0^f$ will be greater than $\mathcal{P}_0^p$ and the BPER $R_e(M,d)$ becomes negative, rendering PPM more battery power-efficient than FSK. Since the $\mathcal{P}_{ct}$ and $\mathcal{P}_{cr}$ threshold for which $R_e(M,d) = 0$ is not analytically tractable, we will resort to a lower bound $\mathcal{P}_{cl}(M,d)$. From (25), we have

$$\begin{aligned} &R_e(M,d) \\ &< 10\log\left(\frac{(\mathcal{E}_s(M,d)\beta+\theta_t\mathcal{P}_{ct})\frac{1}{\mu_{\min}}+\frac{1-a}{a}\cdot\theta_r\mathcal{P}_{cr}\frac{1}{\mu_{\max}}}{(\mathcal{E}_s(M,d)\beta+M\mathcal{P}_{ct})\frac{1}{\mu_{\max}}+\frac{1-a}{a}\cdot M\mathcal{P}_{cr}\frac{1}{\mu_{\max}}}\right) \\ &= 10\log\left(\frac{\mathcal{E}_s(M,d)\beta+\theta\mathcal{P}_c}{\mathcal{E}_s(M,d)\beta+M\mathcal{P}_c}\cdot\frac{\mu_{\max}}{\mu_{\min}}\right). \end{aligned} \tag{26}$$

where $\mathcal{P}_c = \mathcal{P}_{ct} + \frac{1-a}{a}\mathcal{P}_{cr}$, $\theta = \theta_t - \frac{1-a}{a}(\theta_t - \theta_r\frac{\mu_{\min}}{\mu_{\max}})\frac{\mathcal{P}_{cr}}{\mathcal{P}_c}$ and $0 < \theta < 1$ with the assumption of $\frac{\mu_{\min}}{\mu_{\max}} < \theta_t \leq 1$. Notice that so long as $10\log\left(\frac{\mathcal{E}_s(M,d)\beta+\theta\mathcal{P}_c}{\mathcal{E}_s(M,d)\beta+M\mathcal{P}_c}\cdot\frac{\mu_{\max}}{\mu_{\min}}\right) < 0$, it

is guaranteed that $R_e(M,d) < 0$. Hence,

$$\mathcal{P}_c > \mathcal{P}_{cl}(M,d) := \frac{\beta(\mu_{\max}-\mu_{\min})}{\mu_{\min}M-\theta\mu_{\max}} \cdot 2N_0M_lG_1d^K \cdot \ln\left(2\left(1-(1-P_e)^{\frac{1}{M-1}}\right)\right)^{-1}, \forall M,d, \tag{27}$$

where in establishing (27), we used the fact that $\mu_{\min}M \geq 2\mu_{\min} > 1 > \theta\mu_{\max}$. When $\mathcal{P}_c \geq \mathcal{P}_{cl}(M,d)$, we have $R_e(M,d) < 0$ and PPM outperforms FSK. Furthermore, this critical power $\mathcal{P}_{cl}(M,d)$ has the following property:

Lemma 4: *The critical power $\mathcal{P}_{cl}(M,d)$ is a monotonically decreasing function of M for the practical range $P_e \leq 0.0677$; it is also a monotonically increasing function of d, $\forall P_e < 0.5$.*

Proof: The first part can be proved by using the approach in Appendix III. We obtain an upper bound on the derivative of $\mathcal{P}_{cl}(M,d)$:

$$\frac{\partial\mathcal{P}_{cl}(M,d)}{\partial M} \leq \frac{\beta(\mu_{\max}-\mu_{\min})}{(\mu_{\min}M-\theta\mu_{\max})^2} \cdot \left(\frac{2N_0G_d(\mu_{\min}M-\theta\mu_{\max})}{M-1} - E_t(M,d)\right). \tag{28}$$

This upper bound is negative as long as $P_e \leq 0.5e^{\frac{\mu_{\max}\theta}{\mu_{\min}}-2}$. Moreover, $\mu_{\max}/\mu_{\min} > 1$ and $\theta > 0$ imply that $0.5e^{\frac{\mu_{\max}\theta}{\mu_{\min}}-2} > 0.5e^{\theta-2} > 0.5e^{-2} \approx 0.0677$. As a result, we have $\partial\mathcal{P}_{cl}(M,d)/\partial M < 0, \quad \forall P_e \leq 0.0677$. It is worth stressing that even though the SER range $P_e \leq 0.0677$ is indeed practical, it is rather pessimistic. For $\mu_{\max}/\mu_{\min} = 2$ and $\theta \to 1$, the SER range over which $\mathcal{P}_{cl}(M,d)$ is decreasing with M can be extended to $P_e < 0.5$. The second part can be proved by simply inspecting the definition of $\mathcal{P}_{cl}(M,d)$ in (27). □

Based on Lemma 4 and (25), we next compare the battery power efficiency of PPM and FSK:

Proposition 2: *In dense WSNs over Kth power path-loss channels without fading, circuit power consumption $\mathcal{P}_c$ is non-negligible and the following results hold true:*

i) *For any (M,d) pair, there exists a critical power $\mathcal{P}_{cl}(M,d)$ as in (27) such that when $\mathcal{P}_c > \mathcal{P}_{cl}(M,d)$, $R_e(M,d) < 0$ and PPM is more battery power-efficient than FSK.*

ii) *For any given d, if $\mathcal{P}_c > \mathcal{P}_{cl}(2,d)$, then PPM has a power advantage over FSK $\forall M$.*

iii) *For any given d, if $\mathcal{P}_c \leq \mathcal{P}_{cl}(2,d)$, there exists a critical constellation size $M_0 \geq 2$, beyond which PPM has power advantage over FSK $\forall M \geq M_0$.*

iv) *For any given M, there exists a critical distance d_0, within which PPM has power advantage over FSK $\forall d \leq d_0$.*

v) *For small d that makes $\mathcal{P}_c = \mathcal{P}_{ct} + \frac{1-a}{a} \cdot \mathcal{P}_{cr} \gg \mathcal{E}_s(M,d)\beta$, BPER $R_e(M,d) \approx 10\log(\theta'/M)$, and the power advantage of PPM over FSK is very significant for large M.*

Proof: Arguing by construction, $\mathcal{P}_{cl}(M,d)$ ensures that $R_e(M,d) < 0$, $\forall \mathcal{P}_c > \mathcal{P}_{cl}(M,d)$. Furthermore, the first part of Lemma 4 shows that $\mathcal{P}_{cl}(M,d)$ is monotonically decreasing with M; hence, if $\mathcal{P}_c > \mathcal{P}_{cl}(2,d)$, then $\mathcal{P}_c > \mathcal{P}_{cl}(M,d)$, $\forall M$. When $0 < \mathcal{P}_c \leq \mathcal{P}_{cl}(2,d)$, there always exists a unique $M_0 \in [2,-\infty)$ such that $\mathcal{P}_{cl}(M_0,d) \leq \mathcal{P}_c$, $\forall M \geq M_0$. Consequently, $R_e(M,d) < 0$, $\forall M \geq M_0$. Similarly, iv) can be proved based on the second part of Lemma 4. Finally, for small d that makes $\mathcal{P}_c \gg \mathcal{E}_s(M,d)\beta$, the battery discharges linearly so that $\mu(I_t^p(M,d)) \approx \mu(I_t^f(M,d)) \approx 1$. Then BPER $R_e(M,d) \approx 10\log\left(\frac{\mathcal{E}_s(M,d)\beta+\theta_t\mathcal{P}_{ct}+\frac{1-a}{a}\cdot\theta_r\mathcal{P}_{cr}}{\mathcal{E}_s(M,d)\beta+M\mathcal{P}_{ct}+\frac{1-a}{a}\cdot M\mathcal{P}_{cr}}\right) = 10\log(\frac{\mathcal{E}_s(M,d)\beta+\theta'\mathcal{P}_c}{\mathcal{E}_s(M,d)\beta+M\mathcal{P}_c}) \approx 10\log(\theta'/M)$, where $\theta' = \theta_t - \frac{1-a}{a}(\theta_t-\theta_r)\frac{\mathcal{P}_{cr}}{\mathcal{P}_c}$. It takes a large negative value for large M, and thus the power advantage of PPM over FSK is very significant. □

It is worth mentioning that our results derived for path-loss channels subsume the AWGN channel as a special case, by setting the channel gain factor to 1; i.e., $G_d = M_ld^KG_1 = 1$. Then, the transmit energy per symbol $\mathcal{E}_s$, BPER R_e and other power variables become functions of M. Therefore, the results in Proposition 2 with the premise of a fixed d are appropriate for the AWGN channel too.

If the typical linear battery model is applied to battery power efficiency comparisons between PPM and FSK, the battery efficiency factor is $\mu(I) = \mu_{\max}, I \in (I_{\min}, I_{\max})$, instead of (2) and (3). The resulting BPER in the path-loss channel (cf. (25)) is

$$R_e(M,d) = 10\log\left(\frac{\mathcal{E}_s(M,d)\beta+\theta_t\mathcal{P}_{ct}+\frac{1-a}{a}\cdot\theta_r\mathcal{P}_{cr}}{\mathcal{E}_s(M,d)\beta+M\mathcal{P}_{ct}+\frac{1-a}{a}\cdot M\mathcal{P}_{cr}}\right). \tag{29}$$

Obviously, $R_e(M,d) \leq 0, \forall M,d$ and thus PPM is always more power efficient than FSK in dense WSNs, where $\mathcal{P}_{ct} \neq 0$ and $\mathcal{P}_{cr} \neq 0$. In the sparse WSNs, corresponding to $\mathcal{P}_{ct} \to 0$ and $\mathcal{P}_{cr} \to 0$, PPM has the same battery power efficiency as FSK. Comparing these results with those in Proposition 1 and 2, the differences mainly appear in a relatively-long-distance communication, where larger transmit power is needed and the corresponding large discharge current results in non-linear battery power consumption.

So far, we have seen that in path-loss channels, FSK is more battery power-efficient $\forall M,d$ in sparse WSNs with the advantage upper bounded by 3dB; whereas PPM can be more battery efficient in dense WSNs with a more significant power advantage. Next, we will consider Rayleigh fading channels with path-loss effects.

B. Rayleigh Fading Channels with Path-Loss Effects

In Rayleigh fading channels, the transmit energy per symbol for a preset average SER $\bar{P}_e$ is given by (9). When both fading and path-loss effects are considered, the instantaneous channel gain becomes $G = \phi^2/G_d$, where $G_d = M_ld^KG_1$ models the path-loss effect and ϕ is the Rayleigh distributed attenuation factor. Consequently, ϕ^2 is exponentially distributed and $\mathrm{E}\{\phi^2\} = 1$. Hence, the transmit energy per symbol in (9) can be rewritten as

$$\mathcal{E}_s'(M,d) = N_0M_lG_1d^K\left(\left(1-(1-\bar{P}_e)^{\frac{1}{M-1}}\right)^{-1} - 2\right), \tag{30}$$

where the prime $'$ is used to differentiate this subsection's quantities in the presence of fading. As expected, the transmit energy per symbol is again a function of M and d.

B.1. Sparse WSNs: With $\mathcal{P}_c = 0$, the discharge currents for PPM and FSK, as well as their corresponding battery AAPCs have the same form as in (22) and (21), with $\mathcal{E}_s(M,d)$

replaced by $\mathcal{E}'_s(M,d)$. Not surprisingly, we have $R'_e(M,d) = 10\log(\mu(I_t^{f'}(M,d))/\mu(I_t^{p'}(M,d))) > 0$, and the following results:

Proposition 3: *In sparse WSNs over Rayleigh fading channels with path-loss effects, and when circuit power consumption is ignored, results i), iii) and iv) in Proposition 1 hold true. Additionally, with the same (average) SER requirement, we have $R'_e(M,d) > R_e(M,d)$, $\forall M,d$; that is, channel fading induces an increase of the FSK power advantage over PPM.*

Proof: Proving results i), iii) and iv) follows the proof of Proposition 1. We will next prove that $R'_e(M,d) > R_e(M,d)$, $\forall M,d$, when the prescribed average SER $\bar{P}_e$ in fading channels equals the SER P_e in path-loss channels. Since $\partial R_e(M,d)/\partial\mathcal{E}_s(M,d) > 0$ proved in Appendix IV, it suffices to prove that $\mathcal{E}'_s(M,d) > \mathcal{E}_s(M,d)$. With $\bar{P}_e = P_e$, the required energy per symbol in (20) and (30) become:

$$\mathcal{E}_s(M,d) = 2N_0G_d(\ln\left(1-(1-P_e)^{\frac{1}{M-1}}\right)^{-1} - \ln 2),$$
$$\mathcal{E}'_s(M,d) = N_0G_d\left(\left(1-(1-P_e)^{\frac{1}{M-1}}\right)^{-1} - 2\right).$$

Using the inequality $\ln x \le x-1$, it then follows that $\mathcal{E}'_s(M,d) > \mathcal{E}_s(M,d)$. □

Albeit larger, notice that the power advantage of FSK over PPM is still upper bounded by 3dB.

B.2. Dense WSNs: In this case, the discharge currents for PPM and FSK, as well as their corresponding battery AAPCs have the same form as those from (15) to (18), with $\mathcal{E}_s(M,d)$ replaced by $\mathcal{E}'_s(M,d)$. The corresponding BPER is

$$R'_e(M,d) = 10\log\left(\frac{(\mathcal{E}'_s(M,d)\beta+\theta_t\mathcal{P}_{ct})\cdot\frac{1}{\mu(I_t^{p'}(M,d))}+\frac{1-a}{a}\cdot\theta_r\mathcal{P}_{cr}\cdot\frac{1}{\mu_{\max}}}{(\mathcal{E}'_s(M,d)\beta+M\mathcal{P}_{ct})\cdot\frac{1}{\mu(I_t^{f'}(M,d))}+\frac{1-a}{a}\cdot M\mathcal{P}_{cr}\cdot\frac{1}{\mu_{\max}}}\right), \quad (31)$$

and the critical power is

$$\mathcal{P}'_{cl}(M,d) = \frac{\beta(\mu_{\max}-\mu_{\min})}{\mu_{\min}M-\theta\mu_{\max}}\cdot\mathcal{E}'_s(M,d). \quad (32)$$

Proposition 4: *In dense WSNs over Rayleigh fading channels with path-loss effects, results i), iv) and v) in Proposition 2 hold true. Additionally, with the same (average) SER requirement, we have $R'_e(M,d) > R_e(M,d)$, $\forall M,d$.*

Proof: Proving results i), iv) and v) is straightforward given the proof of Proposition 2. In Proposition 3, we have also shown that $\mathcal{E}'_s(M,d) > \mathcal{E}_s(M,d)$, $\forall M,d$. So what is left is to find out whether $\partial R_e(M,d)/\partial\mathcal{E}_s(M,d) > 0$ with $R_e(M,d)$ given by (25). Let us rewrite (25) as

$$R_e = R_{e1} + R_{e2} = 10\log\left(\frac{\mathcal{E}_s\beta+\theta_t\mathcal{P}_{ct}+\frac{1-a}{a}\cdot\frac{\theta_r\mathcal{P}_{cr}}{\mu_{\max}}\mu(I_t^p)}{\mathcal{E}_s\beta+M\mathcal{P}_{ct}+\frac{1-a}{a}\cdot\frac{M\mathcal{P}_{cr}}{\mu_{\max}}\mu(I_t^f)}\right)+10\log\left(\frac{\mu(I_t^f)}{\mu(I_t^p)}\right). \quad (33)$$

Then, differentiation of the first summand R_{e1} yields

$$\frac{\partial R_{e1}}{\partial\mathcal{E}_s} = \frac{10}{\ln(10)}\cdot\left(\frac{\beta+\frac{1-a}{a}\cdot\frac{\theta_r\mathcal{P}_{cr}}{\mu_{\max}}\cdot\frac{\partial\mu(I_t^p)}{\partial\mathcal{E}_s}}{\mathcal{E}_s\beta+\theta_t\mathcal{P}_{ct}+\frac{1-a}{a}\cdot\frac{\theta_r\mathcal{P}_{cr}}{\mu_{\max}}\mu(I_t^p)}-\frac{\beta+\frac{1-a}{a}\cdot\frac{M\mathcal{P}_{cr}}{\mu_{\max}}\cdot\frac{\partial\mu(I_t^f)}{\partial\mathcal{E}_s}}{\mathcal{E}_s\beta+M\mathcal{P}_{ct}+\frac{1-a}{a}\cdot\frac{M\mathcal{P}_{cr}}{\mu_{\max}}\mu(I_t^f)}\right), \quad (34)$$

and that of the second summand R_{e2}

$$\frac{\partial R_{e2}}{\partial\mathcal{E}_s} = \frac{10}{\ln(10)}\left(\frac{\partial\mu(I_t^f)/\partial\mathcal{E}_s}{\mu(I_t^f)}-\frac{\partial\mu(I_t^p)/\partial\mathcal{E}_s}{\mu(I_t^p)}\right). \quad (35)$$

For battery model (2),

$$\frac{\partial\mu(I_t^f)}{\partial\mathcal{E}_s} = -\frac{\nu}{V\eta}\frac{\beta}{M}, \quad \text{and} \quad \frac{\partial\mu(I_t^p)}{\partial\mathcal{E}_s} = -\frac{\nu}{V\eta}\beta. \quad (36)$$

Substituting (36) into (34) and (35), we obtain that $\partial R_{e1}/\partial\mathcal{E}_s > 0$ and $\partial R_{e2}/\partial\mathcal{E}_s > 0$ by the facts that $\mu(I_t^f) > \mu(I_t^p)$ and $\theta_r < 1$, and thus $\partial R_e/\partial\mathcal{E}_s > 0$. For the battery model (3),

$$\frac{\partial\mu(I_t^f)}{\partial\mathcal{E}_s} = -\frac{2\nu}{V\eta}\frac{\beta}{M}I_t^f, \quad \text{and} \quad \frac{\partial\mu(I_t^p)}{\partial\mathcal{E}_s} = -\frac{2\nu}{V\eta}\beta I_t^p. \quad (37)$$

Similarly, by substituting (37) into (34) and (35), we find that $\partial R_e/\partial\mathcal{E}_s = \partial R_{e1}/\partial\mathcal{E}_s + \partial R_{e2}/\partial\mathcal{E}_s > 0$ because $I_t^p > I_t^f$ and $\mu(I_t^f) > \mu(I_t^p)$. □

V. Numerical Results

To confirm our theoretical analysis, we will present quantitative results for Propositions 1-4 by an example of the system shown in Fig. 1(a). The system parameters are listed in Table I. The power supply consists of a generic Li-ion battery with discharge voltage $V = 4.2$V, discharge current with rated maximum $I_{\max} = 10$A and rated minimum $I_{\min} = 0$A, battery efficiency factor with maximum $\mu_{\max} = 1$ and minimum $\mu_{\min} = 0.51$. Then, according to the battery models (2) and (3), we obtain that $\omega = 0.05$ and $\nu = 0.005$. The parameters for the analog circuitry and channels are as in [2], which correspond to general transceivers at 2.5GHz in the Industrial-Scientific-Medical (ISM) band. The power spectral density of the AWGN is $N_0/2 = \sigma^2 = -164$dBm/Hz. A class B power amplifier is used at the transmitter, which makes the drain efficiency $\varsigma = 0.75$. The PAPR is $\xi = 1$ for both FSK and PPM because they have constant modulus during their transmission intervals. Additionally, the proportionality factor between the circuit power consumption for FSK and PPM is $\theta_t = 0.8$ at the transmitter and $\theta_r = 0.95$ at the receiver. With the low data rate and low power setup, we take the bandwidth $B = 10$kHz and symbol error rate $P_e = 10^{-3}$ for both path-loss and fading channels.

First, we consider sparse WSNs. Corresponding to Propositions 1 and 3, Fig. 5 illustrates that the BPER $R_e > 0$ and FSK outperforms PPM $\forall d$ when $M = (2,4,8)$ in both path-loss and fading channels. And the BPER increases as d increases. It can also be verified from the figure that FSK has power advantage over PPM $\forall M$ when d is specified. Moreover, we notice that BPER ≤ 3 dB in sparse WSNs (in our system $\mu_{\max} = 1$ and $\mu_{\min} = 0.51$).

Then, we investigate the power advantage regions of PPM and FSK in dense WSNs. Fig. 6 confirms the existence of critical power $\mathcal{P}_{cl}(M,d)$ and $\mathcal{P}'_{cl}(M,d)$ for all pairs (M,d) as asserted by i) in Propositions 2 and 4, and the monotonically-decreasing properties of $\mathcal{P}_{cl}(M,d)$ over M and d described in Lemma 4. It also shows the PPM and FSK advantage regions over M when $d = 250$m, and over d when $M = 4$ with critical points M_0 and d_0 for the path-loss channel, and d'_0 for the

Battery & Converter	$V = 4.2$ V	$I_{\max} = 10$A	$I_{\min} = 0$A
	$\mu_{\max} = 1$	$\mu_{\min} = 0.51$	$\eta = 0.8$
Modulation & Analog Circuit	$f_c = 2.5$GHz	$\xi = 1$	$\varsigma = 0.75$
	$\mathcal{P}_{syn} = 50$mW	$\mathcal{P}_{filt} = 2.5$mW	$\mathcal{P}_{LNA} = 20$mW
	$\mathcal{P}_{mix} = 30.3$mW	$\mathcal{P}_{IFA} = 3$mW	$\mathcal{P}_{filr} = 2.5$mW
	$\theta_t = 0.8$	$\theta_r = 0.95$	$a = 0.2$
Channel & QoS	$K = 3.0$	$G_1 = 30$dB	$M_l = 40$dB
	$\frac{N_0}{2} = -164$dBm/Hz	$B = 10$KHz	$P_e = 10^{-3}$

TABLE I
SYSTEM PARAMETERS

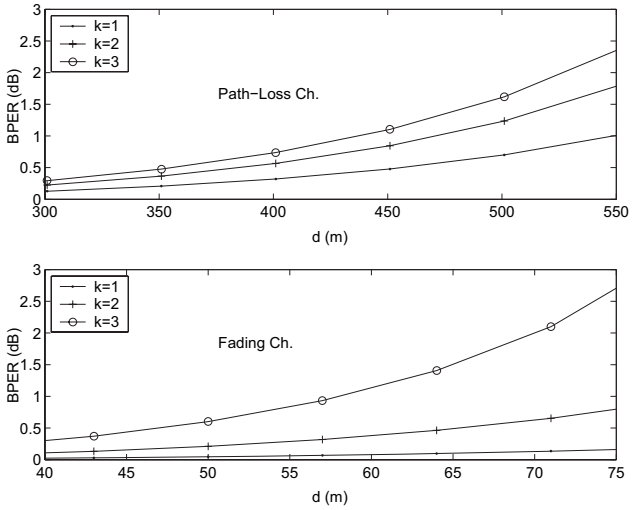

Fig. 5. BPER over transmission distance d with k=1, 2, 3 in sparse WSNs.

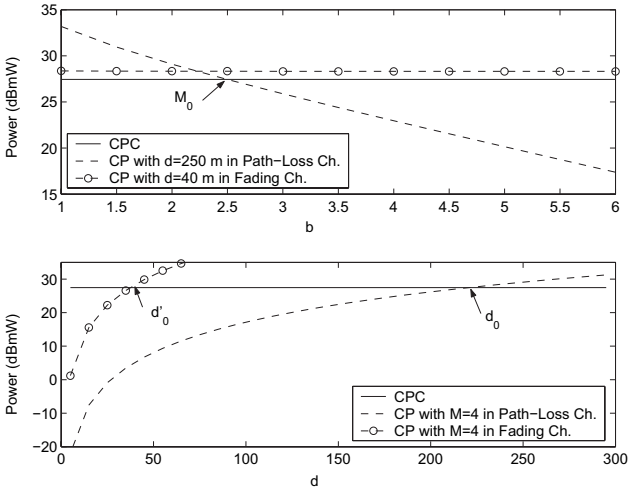

Fig. 6. Circuit power consumption (CPC) $\mathcal{P}_c$, critical power (CP) $\mathcal{P}_{cl}$ and advantage regions for PPM and FSK versus k (Plot 1) and d (plot 2) in dense WSNs.

fading channel;We observe that $\mathcal{P}'_{cl}(M,d) > \mathcal{P}_c\ \forall M$ in the first plot of the figure, which confirms that FSK outperforms PPM $\forall M$ when $d = 40$m in fading channel. What is more, the advantage regions of PPM and FSK can also be shown on the 2D (M, d) plane. They are distinguished by the critical curves $\mathcal{P}_{cl}(M,d) = \mathcal{P}_c$ for the path-loss channel and $\mathcal{P}'_{cl}(M,d) = \mathcal{P}_c$ for the fading channel, which are shown in the first plot of Fig. 7. The area above each critical curve is the advantage region of FSK for the corresponding channel and the areas below them are their advantage regions of PPM. We notice that in very dense WSNs, PPM outperforms FSK $\forall M$ in both channels. It is clear that PPM dominates short-term transmission (dense WSNs) as FSK does in long-term transmission (sparse WSNs). However, both PPM and FSK schemes have limits of maximal transmission distance. These are related to the charge current rated maximum $I_{\max}$ and $\mu_{\min} = \mu(I_{\max})$. The maximal transmission distances for PPM and FSK in both channels can be derived by substituting their related current expressions into (2) or (3); and corresponding numerical results are shown in the second plot of Fig. 7. Obviously, with the same modulation scheme and same system parameters, the maximal transmission distance for the fading channel is much shorter than that for the path-loss channel. The reason is that the required transmit power to achieve the same SER is much greater in fading channel than in path-loss channel.

Finally, we give the BPER numerical values in dense WSNs for both channels. Fig. 8 shows that, in small transmission distance, $d = 30$m in path-loss channel and $d = 5$m in fading channel, their according BPERs $R_e < -15$ dB when $k = 6$ ($M = 64$) and the power advantage of PPM over FSK is very significant, as claimed by v) in Proposition 2 and 4. Also, we observe that $R'_e(M,d) > R_e(M,d)$ for all M when $d = 30$m in the figure, which corroborates the result of Proposition 4.

VI. CONCLUSIONS

In this paper, we have studied and compared the battery energy efficiency of PPM and FSK schemes for a fully-functioning node, where the battery power consumption is closely related to the transmit power, analog circuit power consumption during transmission and reception modes and battery non-linearity. The results reveal interesting properties of PPM and FSK with respect to battery power efficiency, dependence on the sensor node distribution, modulation constellation size and the type of the wireless channel. Specifically, in sparse WSNs with negligible circuit power consumption, FSK has power efficiency advantage over PPM for all constellations of any size M and transmit distance d in path-loss and fading channels; the advantage in fading channels is greater than that in path-loss channels; and the advantage is no more than 3 dB. However, when transmission distance decreases and the circuit power consumption is comparable to the transmit power, PPM and FSK have their respective advantage regions: PPM is more energy-efficient at relatively higher data rates and/or denser sensor deployments; and the advantage of PPM over FSK in path-loss channels is greater than that in fading channels; In

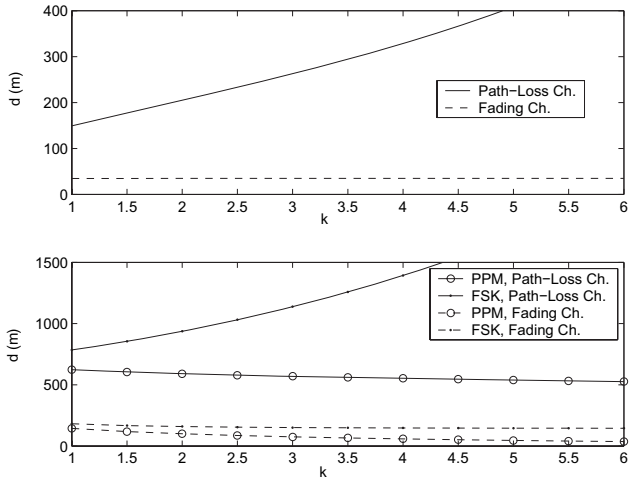

Fig. 7. Critical curves for PPM and FSK advantage regions on (M,d) plane (plot 1) and maximal transmission distances for PPM and FSK over k (plot 2) in dense WSNs.

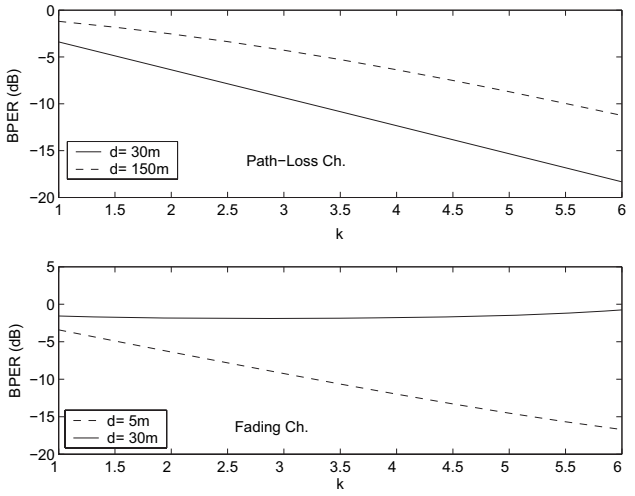

Fig. 8. BPER versus k in dense WSNs.

very dense WSNs, when circuit power consumption dominates the total power consumption of sensors, PPM outperforms FSK over all M and exhibits a big advantage, especially for large M.

APPENDIX I
PROOF OF LEMMA 1

With non-coherent energy detection, the SER of equi-probable M-ary orthogonal modulations is [14, Chap. 5]: $P_e = \int_0^\infty (1-(1-e^{-x^2/2})^{M-1}) f(x)dx$, where $f(x) = xe^{-(x^2+2\gamma)/2} I_0(\sqrt{2\gamma x})$ is the Rice probability distribution function and $\gamma = G\mathcal{E}_s/N_0$ is the receive SNR. Since $1-(1-y)^{M-1}$ is a concave function on $y \in [0,1]$, Jensen's inequality implies that $\mathrm{E}\{1-(1-y)^{M-1}\} \le 1-(1-\mathrm{E}\{y\})^{M-1}$. Setting $y = e^{-\frac{x^2}{2}}$, we obtain

$$\begin{aligned} P_e &= 1-\int_0^\infty \left(1-e^{-\frac{x^2}{2}}\right)^{M-1} f(x)dx \\ &\le 1-\left(1-\int_0^\infty e^{-\frac{x^2}{2}} f(x)dx\right)^{M-1} = 1-\left(1-\tfrac{1}{2}e^{-\frac{\gamma}{2}}\right)^{M-1}. \end{aligned} \tag{38}$$

Next, we will show that the bound in (38) is tighter than the union bound; that is

$$1-\left(1-\frac{1}{2}e^{-\frac{\gamma}{2}}\right)^{M-1} \le (M-1)\frac{1}{2}e^{-\frac{\gamma}{2}}, \quad \forall M \ge 2,\ \gamma \ge 0. \tag{39}$$

As function $1-(1-y)^{M-1}$ is concave on $y \in [0,1]$, it is always upper bounded by its tangent line passing through point (0,0); i.e., $1-(1-y)^{M-1} \le (M-1)y$. Setting $y = e^{-\frac{\gamma}{2}}$ leads to (39).

APPENDIX II
PROOF OF LEMMA 2

In Rayleigh fading channels, the channel gain G is a variant with exponential distribution. Then $\gamma = G\mathcal{E}_s/N_0$ follows to be exponentially-distributed: $f(\gamma) = (1/\bar{\gamma})e^{-\gamma/\bar{\gamma}}$ with $\bar{\gamma} := \mathrm{E}\{G\mathcal{E}_s/N_0\} = \bar{G}\mathcal{E}_s/N_0$. Using (38), we have:

$$\begin{aligned} \bar{P}_e &= \int_0^\infty P_e(\gamma) f(\gamma) d\gamma \\ &\le \int_0^\infty \left(1-\left(1-\tfrac{1}{2}e^{-\frac{\gamma}{2}}\right)^{M-1}\right) \cdot \tfrac{1}{\bar{\gamma}} e^{-\frac{\gamma}{\bar{\gamma}}} d\gamma \\ &= 1-\left(1-\tfrac{1}{2+\bar{\gamma}}\right)^{M-1}. \end{aligned}$$

APPENDIX III
PROOF OF LEMMA 3

By definition, the required energy per symbol is:

$$\begin{aligned} \mathcal{E}_s(M,d) &= -2N_0 G_d \ln\left(2\left(1-(1-P_e)^{\frac{1}{M-1}}\right)\right) \\ &= -2N_0 G_d \ln\left(2\left(1-P_c^{\frac{1}{M-1}}\right)\right), \end{aligned} \tag{40}$$

where $P_c := 1-P_e$ is the probability of correctly decoding a symbol. Differentiating, we find

$$\frac{\partial \mathcal{E}_s(M,d)}{\partial M} = 2N_0 G_d \frac{P_c^{\frac{1}{M-1}}}{1-P_c^{\frac{1}{M-1}}} \cdot \frac{-\ln P_c}{(M-1)^2} > 0, \tag{41}$$

where to establish the inequality, we used the fact that $0 < P_c < 1$. Eq. (41) proves that $\mathcal{E}_s(M,d)$ is an increasing function of M. Next, we will show that $\partial\mathcal{E}_s(M,d)/\partial M$ is upper bounded by $2N_0G_d/(M-1)$, $\forall M > 1$. To this end, we notice first that

$$\begin{aligned} &\tfrac{\partial}{\partial P_c}\tfrac{\partial \mathcal{E}_s(M,d)}{\partial M} \\ &= 2N_0 G_d \frac{P_c^{\frac{2-M}{M-1}}}{(M-1)^2\left(1-P_c^{\frac{1}{M-1}}\right)^2}\left(P_c^{\frac{1}{M-1}} - 1 - \ln P_c^{\frac{1}{M-1}}\right) \ge 0, \end{aligned}$$

where the equality holds if and only if $P_c = 1$. We hence obtain the following bound (cf. (41)):

$$\frac{\partial \mathcal{E}_s(M,d)}{\partial M} \le \lim_{P_c \to 1} \frac{\partial \mathcal{E}_s(M,d)}{\partial M} = \frac{2N_0 G_d}{M-1}.$$

Based on this upper bound, we find that

$$\begin{aligned} \tfrac{\partial}{\partial M}\tfrac{\mathcal{E}_s(M,d)}{M} &= \tfrac{1}{M^2}\left(M\tfrac{\partial \mathcal{E}_s(M,d)}{\partial M} - \mathcal{E}_s(M,d)\right) \\ &\le \tfrac{1}{M^2}\left(\tfrac{2N_0 G_d M}{M-1} - \mathcal{E}_s(M,d)\right). \end{aligned}$$

Using the definition of $\mathcal{E}_s(M,d)$ in (40), it can be shown that the right-hand side of the above equation is negative so long as $P_c \ge P(M) = \left(1-e^{-M/(M-1)}/2\right)^{M-1}$, $\forall M \ge 2$.

Moreover, the upper bound $P(M)$ is maximized at $M = 2$ because

$$\frac{\partial \ln P(M)}{\partial M} = \ln\left(1 - \frac{e^{\frac{-M}{M-1}}}{2}\right) - \frac{1}{2 - e^{\frac{-M}{M-1}}} \cdot \frac{1}{M-1} \cdot e^{\frac{-M}{M-1}} < 0 .$$

Consequently, we have

$$\frac{\partial}{\partial M}\frac{\mathcal{E}_s(M,d)}{M} < 0, \quad \forall M \geq 2, \tag{42}$$

as long as $P_c \geq P(2) \approx 0.9323$. In other words, over the practical SER range $P_e \leq 0.0677$, $\mathcal{E}_s(M,d)/M$ is a decreasing function of M.

APPENDIX IV
PROOF OF PROPOSITION 1

Since $I_t^p(M,d) > I_t^f(M,d)$ (cf. (22)) and $\mu(I_t)$ is a monotonically decreasing function of I_t (cf. (2) and (3)), we have $\mu(I_t^f(M,d)) > \mu(I_t^p(M,d))$ and accordingly $R_e(M,d) > 0$. Thus, the battery AAPC of FSK is always smaller than that of PPM.

To prove that $R_e(M,d)$ is an increasing function of M, we start from its definition in (23). With the battery models (2) and (3), we have respectively:

$$R_e(M,d) = 10\log\left(\frac{\mu(I_t^f(M,d))}{\mu(I_t^p(M,d))}\right) = 10\log\left(\frac{1-\omega\cdot\frac{\beta}{V\eta}\cdot\frac{\mathcal{E}_s(M,d)}{M}}{1-\omega\cdot\frac{\beta}{V\eta}\cdot\mathcal{E}_s(M,d)}\right)$$

and

$$R_e(M,d) = 10\log\left(1-\nu\left(\frac{\beta}{V\eta}\cdot\frac{\mathcal{E}_s(M,d)}{M}\right)^2\right) - 10\log\left(1-\nu\left(\frac{\beta}{V\eta}\cdot\mathcal{E}_s(M,d)\right)^2\right).$$

In both cases, $\mathcal{E}_s(M,d)/M$ appears in the numerator while $\mathcal{E}_s(M,d)$ appears in the denominator. Based on (41) and (42), we deduce that $R_e(M,d)$ increases monotonically with M for both battery models.

Then, for any given M, we will prove that $R_e(M,d)$ is an increasing function of d. As the only d-dependent term in $R_e(M,d)$ is $\mathcal{E}_s(M,d)$, it suffices to apply the chain rule: $\frac{\partial R_e(M,d)}{\partial d} = \frac{\partial R_e(M,d)}{\partial \mathcal{E}_s(M,d)} \cdot \frac{\partial \mathcal{E}_s(M,d)}{\partial d}$. With battery models (2) and (3), we have respectively (cf. (23)):

$$\frac{\partial R_e(M,d)}{\partial \mathcal{E}_s(M,d)} = \begin{cases} \frac{10}{\ln(10)} \cdot \frac{(M-1)\ \mu(I_t^p(M,d))}{M\ \mu(I_t^f(M,d))} \cdot \frac{\omega\lambda}{(1-\omega\lambda\mathcal{E}_s(M,d))^2}, \\ \frac{10}{\ln(10)} \cdot \frac{(M^2-1)\ \mu(I_t^p(M,d))}{M^2\ \mu(I_t^f(M,d))} \cdot \frac{2\nu\lambda^2\mathcal{E}_s(M,d)}{(1-\nu\lambda^2\mathcal{E}_s^2(M,d))^2}, \end{cases} \tag{43}$$

where $\lambda := \beta/(V\eta)$ is a constant. Evidently, Eq. (43) is positive for both cases. Furthermore, the derivative $\frac{\partial \mathcal{E}_s(M,d)}{\partial d} > 0$, $\forall P_e < 0.5$ can be readily obtained from its definition (20). Therefore, for any given M, the BPER $R_e(M,d)$ is an increasing function of d.

The upper bound of BPER can be obtained based on the intrinsic property of batteries as follows $R_e(M,d) = 10\log\left(\frac{\mu(I_t^f(M,d))}{\mu(I_t^p(M,d))}\right) \leq 10\log\left(\frac{\mu_{\max}}{\mu_{\min}}\right)$. Since $\mu_{\max} = 1$ and $\mu_{\min} > 0.5$, the upper bound turns out to be 3dB.

REFERENCES

[1] I. F. Akyildiz *et al.*, "Wireless sensor networks: a survey," *Computer Networks (Elsevier) Journal*, vol. 38, no. 4, pp. 393-422, Mar. 2002.

[2] S. Cui, A. J. Goldsmith, and A. Bahai, "Energy-Constranined Modulation Optimization," *IEEE Trans. Wireless Commun.*, vol. 4, no. 5, pp. 2349-2360, Sept. 2005.

[3] A. J. Goldsmith and S. B. Wicker, "Design Challenges for Energy-Constrained Ad Hoc Wireless Networks," *IEEE Wireless Commun. Mag.*, vol. 9, no. 4, pp. 8-27, Aug. 2002.

[4] L. van Hoesel *et al.*, "Prolonging the lifetime of wireless sensor networks by cross-layer interaction," *IEEE Wireless Commun. Mag.*, vol. 11, no. 6, pp. 78-86, Dec. 2004.

[5] L. W. Hughes, "A Simple Upper Bound on the Error Probability for Orthogonal Signals in White Noise," *IEEE Trans. Commun.*, vol. 40, no. 4, pp. 670, Apr. 1992.

[6] K. Lahiri *et al.*, "Battery-Driven System Design: A New Frontier in Low Power Design," in *Proc. Int'l. Conf. VLSI Design*, Bangalore, India, Jan. 2002, pp. 261-267.

[7] J. N. Laneman, D. N. C. Tse, and G. W. Wornell, "Cooperative Diversity in Wireless Networks: Efficient Protocols and Outage Behavior," *IEEE Trans. Inform. Theory*, vol. 50, no. 12, pp. 3062-3080, Dec. 2004.

[8] T. H. Lee, *The Design of CMOS Radio-Frequency Integrated Circuits*, Cambridge University Press, Cambridge, U.K., 1998.

[9] T. L. Martin and D. P. Siewiorek, "Nonindeal Battery Properties and Their Impact on Software Design for Wearable Computers," *IEEE Trans. Computers*, vol. 52, no. 8, pp. 979-984, Aug. 2003.

[10] D. Panigrahi *et al.*, "Battery Life Estimation of Mobile Embedded Systems," in *Proc. 14th Int'l. Conf. on VLSI Design*, Jan. 2001, pp. 57-63.

[11] M. Pedram and Q. Wu, "Design Considerations for Battery-Powered Electronics," in *Proc. 36th ACM/IEEE Conf. on Design Automation,* New Orleans, Louisiana, USA, June 1999, pp. 861-866.

[12] J. Polastre *et al.*, "The Mote Revolution: Low Power Wireless Sensor Network Devices," Sept. 2004, available at http://webs.cs.berkeley.edu/papers/hotchips-2004-motes.ppt

[13] Y. Prakash and S. K. S. Gupta, "Energy Efficient Source Coding and Modulation for Wireless Applications," in *Proc. Wireless Comm. & Networking Conf.*, New Orleans, Louisiana, USA, Mar. 2003, pp. 212-217.

[14] J. G. Proakis, *Digital Communications, 4th Edition*. New York: McGraw-Hill, 2000.

[15] D. Rakhmatov and S. Vrudhula, "Time to Failure Estimation for Batteries in Portable systems," in *Proc. Int'l. Symp. on Low Power Electr. & Design*, Huntington Beach, CA, USA, Aug. 2001, pp. 88-91.

[16] D. Rakhmatov and S. Vrudhula, "Energy Management for Battery-Powered Embedded Systems," *ACM Trans. Embedded Comp. Systems*, vol. 2, pp. 277-324, Aug. 2003.

[17] A. Y. Wang *et al.*, "Energy Efficient Modulation and MAC for Asymmetric RF Microsensor Systems," in *Proc. Intl. Symp. Low Power Electr. & Design*, Huntington Beach, CA, USA, Aug. 2001, pp. 106-111.

Qiuling Tang received her B.S. degree in Electrical Engineering from National University of Defense Technology, Changsha, China, in 1990. Since then, she is with Guangxi University, Nanning, China, where she received her postgraduate diploma in Computer science and engineering in 2002, and became an associate professor in 2004. From October 2003 to January 2005 she worked in West Virginia University and University of Minnesota as a visiting researcher. Currently, She is also a doctorial candidate in Nanjing University, Nanjing, China. Her research interests include digital communication, signal processing and networking. Presently, she focuses on wireless sensor networks, CDMA wireless systems and information security.

Liuqing Yang (M'04) received her B.S. degree in Electrical Engineering from Huazhong University of Science and Technology, Wuhan, China, in 1994, and her M.Sc. and Ph.D. degrees in Electrical and Computer Engineering from the University of Minnesota, Minneapolis, in 2002 and 2004, respectively. Since August 2004, she has been an assistant professor with the Department of Electrical and Computer Engineering at the University of Florida, Gainesville. Her research interests include communications, signal processing and networking. Her current research encompasses synchronization, channel estimation, equalization, multiple access, space-time coding, multi-carrier wireless systems and ultra-wideband communications.

Georgios B. Giannakis (F97) received his Diploma in Electrical Engr. from the Ntl. Tech. Univ. of Athens, Greece, 1981. From 1982 to 1986 he was with the Univ. of Southern California (USC), where he received his MSc. in Electrical Engineering, 1983, MSc. in Mathematics, 1986, and Ph.D. in Electrical Engr., 1986. Since 1999 he has been a professor with the ECE Department at the Univ. of Minnesota, where he now holds an ADC Chair in Wireless Telecommunications. His general interests span the areas of communications, networking and statistical signal processing - subjects on which he has published more than 250 journal papers, 450 conference papers, two edited books and two research monographs. Current research focuses on diversity techniques, complex-field and space-time coding, multicarrier, cooperative wireless communications, cognitive radios, cross-layer designs, mobile ad hoc networks, and wireless sensor networks. G. B. Giannakis is the (co-) recipient of six paper awards from the IEEE Signal Processing (SP) and Communications Societies including the G.Marconi Prize Paper Award inWireless Communications. He also received Technical Achievement Awards from the SP Society (2000), from EURASIP (2005), a Young Faculty Teaching Award and the G. W. Taylor Award for Distinguished Research from the University of Minnesota. He has served the IEEE in a number of posts.

Tuanfa Qin received his B.S. and his M.Sc. degrees in Physics from Guangxi University, Nanning, China, in 1988 and 1991, respectively, and his Ph. D. degree in Acoustics from Nanjing University, Nanjing, China, in 1997. Since 1991, he is with Guangxi University, Nanning, China, where he became a professor of Electrical Engineering in 2001. Since 2002, he is also a professor in Nanjing University, Nanjing, China. His general interests is digital communication, signal processing, cryptology and networking security. Up to now, he has published more than 80 journal papers and one edited book. His current research focuses on wireless multimedia communication, CDMA system and stream cipher.